Chinese Chemical Letters 36 (2025) 110816

Contents lists available at ScienceDirect

Chinese Chemical Letters

journal homepage: www.elsevier.com/locate/cclet

Decouple the intermolecular interaction by encapsulating an insulating sheath

Saisai Yuan[a,b], Yiming Chen[a], Xijuan Wang[a], Degui Zhao[c], Tengyang Gao[c,d,*], Caiyun Wei[e], Chuanxiang Chen[a], Yang Yang[e,*], Wenjing Hong[e,*]

[a] School of Environmental and Chemical Engineering, Jiangsu University of Science and Technology, Zhenjiang 212100, China
[b] National & Local Joint Engineering Research Center for Mineral Salt Deep Utilization, Huaiyin Institute of Technology, Huaian 223003, China
[c] Key Laboratory of Organic Compound Pollution Control Engineering (MOE), School of Environmental and Chemical Engineering, Shanghai University, Shanghai 200444, China
[d] College of Chemical Engineering & College of Materials Science and Engineering, Fuzhou University, Fuzhou 350108, China
[e] State Key Laboratory of Physical Chemistry of Solid Surfaces, College of Chemistry and Chemical Engineering & Pen-Tung Institute of Micro-Nano Science and Technology, Xiamen University, Xiamen 361005, China

ARTICLE INFO

Article history:
Received 26 August 2024
Revised 26 December 2024
Accepted 2 January 2025
Available online 2 January 2025

Keywords:
Single-molecule
Molecule devices
Host-guest interaction
Confinement effect
Decouple

ABSTRACT

Single-molecule junctions are building blocks for constructing molecular devices. However, intermolecular interactions like winding bring additional interference among the surrounding molecules, which inhibits the intrinsic coherent transport through single-molecule junctions. Here, we employed a nanocavity (dimethoxypillar[5]arene, DMP[5]), which is analogous to electric cables, to confine the conformation of flexible chains (1,8-diaminooctane, DAO) *via* host-guest interaction. Single-molecule conductance measurements indicate that the conductance of DAO encapsulated with DMP[5] is as high as that of pure DAO, as reproduced by theoretical simulations. Intriguingly, the molecular lengths of the DAO encapsulated with DMP[5] increase from 1.13 nm to 1.46 nm compared with the pure DAO, indicating that DMP[5] keeps DAO upright-standing *via* the confinement effect. This work provides a new strategy to decouple the intermolecular interaction by employing an insulating sheath, enabling the high-density integration of single-molecule devices.

© 2025 Published by Elsevier B.V. on behalf of Chinese Chemical Society and Institute of Materia Medica, Chinese Academy of Medical Sciences.

Molecular electronics provide the potential for manufacturing next-generation electronic devices. The advances [1–7] in building single-molecule junctions have enabled the investigation of molecular materials at the single-molecule level, revealing their potential physicochemical properties [8–14]. However, to apply single-molecule junctions to electronic devices [15,16], high-density integration of single-molecule junctions remains challenging due to the significant effect on the intrinsic transport properties among the extremely close molecular junctions [17,18]. For instance, the rotation of benzene rings changes the conjugation property of molecules and significantly changes the conductance of molecular junctions [19]. In addition, the configurations of molecular junctions constructed by long and flexible molecules generate significant change with the external stimuli [20–22] causing the instability of molecular devices.

Alkyl chains are widely used in single-molecule [23–25] and monolayer [26,27] devices because of their stable chemical and tunable electrical properties [20]. However, the flexibility, intermolecular interactions of alkyl chains and alkane/Au van der Waals contact, such as winding and folding, induced an uncertain configuration at the single-molecule level [25,28–30], led to the submersion of the intrinsic electric transport properties and limit high-density integration implementation. In previous studies, Hu *et al.* [31]. inserted saturated hydrocarbon fragments between the anchoring group and the backbone to decouple the ferrocene and electrodes. In addition, recent works show that the saturated alkane still owns the σ-σ stacked supramolecular interaction [32,33], which influences the intrinsic electric transport properties. Very recently, Lucia *et al.* [34]. found a similar phenomenon that the host-guest complex could prevent the formation of π-π stacked dimers and permit the determination of the single-molecule conductance without intermolecular charge transport. However, it remains challenging to encapsulate protective layers on alkyl-chain molecules and stabilize the molecular junction

* Corresponding authors.
E-mail addresses: tygao@shu.edu.cn (T. Gao), yangyang@xmu.edu.cn (Y. Yang), whong@xmu.edu.cn (W. Hong).

https://doi.org/10.1016/j.cclet.2025.110816
1001-8417/© 2025 Published by Elsevier B.V. on behalf of Chinese Chemical Society and Institute of Materia Medica, Chinese Academy of Medical Sciences.

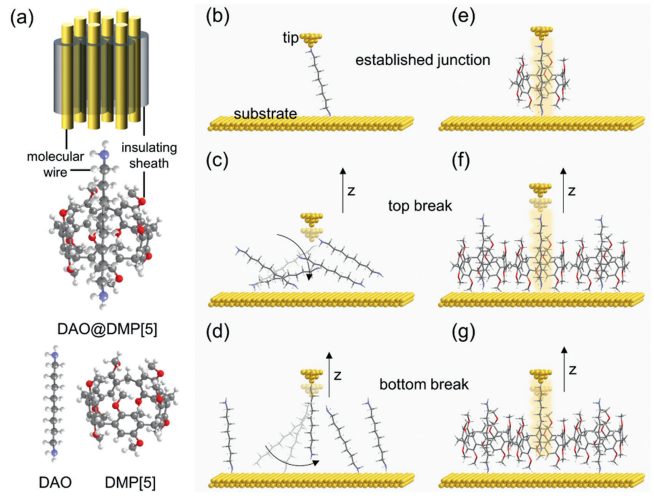

Fig. 1. (a) The schematics of the molecular cables, the chemical structures of DAO, DMP[5] and DAO@DMP[5] complex. white: hydrogen, blue: nitrogen, grey: carbon, red: oxygen. Diagrams of molecular junction breaking of DAO (b-d) and DAO@DMP[5] (e-g) complex at the single-molecule scale, respectively. The upper represents the tip and the bottom represents the substrate. (b, e) is the schematic diagram of established molecular junctions. In the process of pulling, when the molecular junction is not fully unfolded, (c, f) is broken from the point of connection with the tip, and (d, g) is broken from the point of connection with the substrate.

at a fully stretched state effectively at the single-molecule level [35–37].

Herein, we employed the host-guest interaction to encapsulate DAO molecule. We wrapped a shielding layer around the molecular wire using dimethoxypillar[5]arene (DMP[5]) to inhibit intermolecular interaction and stabilize the molecular junction of DAO@DMP[5] complex. DMP[5] was employed because of the following considerations. First, DMP[5] represent a group of cyclic compounds composed of aromatic benzene rings and their derivative units were connected by methylene bridges, which make them special in chemical reactions and molecular recognition [38]. Second, DMP[5] have electron-rich hydrophobic cavities with adjustable sizes, which can interact with the molecules of different sizes and shapes to achieve selective recognition and separation [39,40]. Third, the structure of DMP[5] can be modified by introducing functional groups into its side chain and terminal, and specific host-guest complex properties can be obtained. Finally, DMP[5] can self-assemble to form unique supramolecular structures under appropriate conditions, such as nanotubes, nanosheets, micelles [41–45]. In this work, DMP[5] molecule served as the shielding layer in the conventional cable. It inhibited the intermolecular interaction and the folding and winding of the alkyl chains. The increment of length of DAO@DMP[5] complex indicated that DMP[5] kept DAO upright-standing *via* the confinement effect. The nearly identical conductance of pure DAO molecule and assembled DAO@DMP[5] complex were also confirmed by theoretical calculations. Our work provides a new strategy for decoupling intermolecular interactions based on host-guest effects and is expected to be applied to improve the high-density integration of single-molecule devices.

As shown in Fig. 1a, the macrocyclic molecules serve as the insulating sheath to protect the alkyl chains from folding or intertwining, which can be realized in a classical host-guest supramolecular primitive model. Briefly, we used the scanning tunneling microscope break junction (STM-BJ) technique [46] to construct a single-molecule junction and choose DMP[5] molecule as an insulating sheath to decouple the intermolecular interaction of alkyl chains. The hydrogen spectrum nuclear magnetic (^{1}H NMR) information of DMP[5] was detailed in Fig. S1 (Supporting information). The ^{1}H NMR, 2D NOESY NMR and high-resolution mass spectrum also confirm that there is a significant host-guest interaction between DAO and DMP[5] (Figs. S2 and S3 in Supporting information). The STM-BJ setup diagram was shown in Fig. S4 (Supporting information). We demonstrated that encapsulated molecular wires not only kept the long alkyl chain upright-standing and fully stretched but also inhibited the interaction between molecules through the molecular confinement and obtained the intrinsic molecular properties.

DMP[5] and DAO can form the host-guest complex identified by previous work [47]. As shown in Fig. 1a, the space of the DMP[5] nanocavity can only accommodate one DAO molecule. And the length of the DOA matched the cavity depth of the DMP[5], ensuring the exposure of the anchoring groups. Previous works have indicated that the alkyl-chain junctions own variable conformations due to their flexibility and alkane/Au van der Waals contact [30], leading to the declining and folding [25,28,48] molecular junctions. In addition, we calculated the binding energies between DAO molecules. An interaction between DAO dimers was confirmed by the negative binding energies of three types of configurations (Figs. S10a-c in Supporting information). Therefore, there is a probability that the DAO molecules are unable to upright-standing by themselves or fully stretched due to their long molecular length and intermolecular interaction, as shown in Fig. 1b. In the process of lifting the tip, there are two breaking modes, 'top break' and 'bottom break'. As shown in Fig. 1c, one mode is that molecular connections break off from the tip. Another mode is shown in Fig. 1d, the molecules disconnect from the substrate. For the assembled DAO@DMP[5] complex molecules, the break junction process was shown in Fig. 1e. The DAO was encapsulated with DMP[5], which keeps DAO upright-standing and inhibits intermolecular interaction. Therefore, no matter what type of breaking (Figs. 1f and g), the stretched length is mostly the maximum length of the molecular junction. Therefore, the stretching length of the DAO@DMP[5] complex should be longer than that of the individual DAO due to the decoupling effect from DMP[5], which is expected to be observed from the displacement distributions in single-molecule conductance measurement.

To investigate the stretching length of individual DAO and DAO@DMP[5] complex, the experimental conditions of single-molecule measurement were kept the same, including the stretching rate, concentration and applied bias voltage. The mixed solvent was the 10 vol% dichloromethane (DCM) and 90 vol% mesitylene (TMB). Furthermore, 0.1 V bias voltage was applied between the tip and substrate in the single-molecule conductance measurements. A sharp peak around 1 G_0 comes from the formation of Au-Au atomic point contacts [49], G_0 was the quantum conductance (where $G_0 = 77.6$ μS) [10]. As shown in Fig. S5 (Supporting information), no conductance signal was observed for the pure solvent and pure DMP[5], indicating that DAO dominated conductance in subsequent measurement. As shown in Fig. 2a, one-dimensional (1D) conductance histograms of individual DAO, individual DMP[5] and DAO@DMP[5] complex were constructed, respectively. There was no discernable signal in individual DMP[5], indicating that the conductance originated from DAO due to its bilateral amino groups. In addition, we noticed that the conductance value of the complex formed by the assembly of DAO and DMP[5] molecules did not change significantly, but the conductance peak characteristics of DAO@DMP[5] complex showed a widening phenomenon. To further reveal this phenomenon, we studied the individual conductance traces corresponding to the three molecules in Fig. 2a. As shown in Fig. 2b, DMP[5] had no significant conductance signal, and the single curves of the individual DAO were similar as previous studies. An interesting observation was that there was a ap-

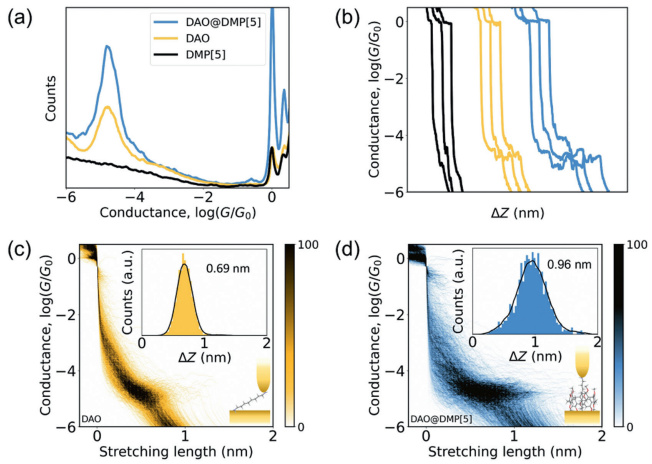

Fig. 2. Measurements of single-molecule conductance. (a) 1D conductance histograms at 0.1 V bias voltage and (b) the individual conductance traces. (c) 2D conductance-displacement histograms of DAO molecule, the insets are the displacement distribution and scheme of DAO molecular junction, (d) 2D conductance-displacement histograms of DAO@DMP[5] complex, the insets are the displacement distribution and schematics of DAO@DMP[5] complex molecular junction. The corresponding relative displacement distribution of single-molecule junctions, which were calibrated with conductance region from $10^{-2.0}$ G_0 to $10^{-6.0}$ G_0 (775 nS to 0.08 nS), respectively.

parent difference in stretching length between individual DAO and DAO@DMP[5] complex, with at least one seems to showed transitions between two distinct plateau. This might be the shielding effect of DMP[5] molecule, which made DAO molecule more inclined to the stretched upright state, resulting in a longer plateau and the broadening of conductance peak.

To study the stretching lengths of individual DAO and DAO@DMP[5] complex, single-molecule conductance data were converted to a 2D histograms. As shown in Figs. 2c and d, we overlapped approximately 2000 such individual conductance traces to form the 2D conductance histograms and corresponding displacement distribution histograms. The 2D conductance histograms had shapes similar to those of the individual conductance traces in the corresponding ranges. Additionally, the shape of 2D conductance histograms from pure DAO was inclined, indicating the existence of a sliding process of Au electrodes on molecules. While for the DAO@DMP[5] complex, the shape of 2D conductance histograms was very flat, indicating that the connection and disconnection of molecular junctions occurred in an upright state. As shown in the insets of Figs. 2c and d, considering the Au-Au snapback distance (0.50 nm) after the rupture of Au-Au atomic point contacts [50], the stretching lengths for the individual DAO and DAO@DMP[5] complex were about 1.13 nm (0.63 nm plus 0.50 nm) and 1.46 nm (0.96 nm plus 0.50 nm), respectively. The theoretical length of DAO@DMP[5] complex was calculated to be 1.13 nm (Fig. S9 in Supporting information). After accounting for the length of two Au-N bonds (0.44 nm), the final length was determined to be 1.57 nm (1.13 nm plus 0.44 nm). This closely aligned with the experimental value of DAO@DMP[5] complex (1.46 nm), indicating that the molecular junction of DAO@DMP[5] complex were almost fully stretched. Interestingly, we found that the stretching length of the molecular junction constructed between the tip and substrate did not reach the maximum initially, but it changed gradually with time during the measurement. We inferred that DAO and DMP[5] molecules progressively assembled with the extension of measurement time. The configuration of the molecular junction formed with individual DAO was significantly different from that formed with DAO@DMP[5] complex, thus changing the stretching length.

The assembly process of complex can be characterized by NMR, UV–vis and fluorescence spectroscopy *etc.* at present. However, the characterization results of these technique are the average behavior of a large number of molecules, which cannot reveal the microscopic dynamic information of an individual molecule at the single-molecule level [51]. STM-BJ can reflect the dynamic structure changes of single-molecule junction through different conductance signals, thus providing a reliable research platform for real-time detection of changes in the dynamic molecular assembly process. We investigated the assembly process of DAO and DMP[5] molecules by collecting and counting the conductance signals at 5-min intervals (Fig. S11 in Supporting information). As shown in Figs. 3a-e, we analyzed the successive groups of data by 2D conductance-displacement histograms at 0.1 V bias voltage and the 1D conductance histograms were shown in Fig. S6 (Supporting information). The values of conductance of DAO@DMP[5] complex were approaching while the stretching lengths increased over time. However, the stretching lengths of individual DAO remained constant (Fig. S7 in Supporting information), which provided evidence of interaction between DAO and DMP[5] molecules. These results indicated that the configuration of the DAO molecular junction changed with the assembly. We further plotted the relationship between stretching length and measurement time with the results of Figs. 3a-e, as shown in Fig. 3f. For the DAO molecular junction, its stretching length was almost unchanged. The stretching length of the DAO@DMP[5] complex junction increased with the measurement time, indicating that the proportion of host-guest assemblies increased gradually and the assembly improved the stability of molecular junctions. The increase in stretching length stopped at the Group 5, then reached a dynamic equilibrium.

To further study the charge transport property and stability, we performed the flicker noise analysis [52,53]. The correlation between noise power and average conductance can be used to determine the transport type and stability of molecular junction qualitatively. More information on the power spectral density (PSD) experiments can be found in previous reports [54], and details are provided in the methods. The charge transport properties of the molecule-electrode interface depend on the interaction between molecule and electrode, and the noise can be used as one of the parameters to evaluate it. The noise power is proportional to G^n, where n is an index indicating the type of molecule-electrode coupling. As n approaches 1.0, the charge transport tends to 'through-bond'. As n approaches 2.0, the charge transport is mainly by the 'through-space'. As shown in Figs. S8a and c (Supporting information), individual DAO molecule showed that noise power was sensitive to the change of conductance and the corresponding noise power scale was 2.0, indicating that the charge transport was through-space mechanism. For the DAO@DMP[5] complex, the corresponding noise power scale was 1.4 (Figs. S8b and d in Supporting information), indicating that the charge transport tended to the through-bond way. The fluctuation of noise power of DAO@DMP[5] complex was suppressed, resulting from the enhanced stability of the host-guest assembly on the molecular junction.

To explore the influence of DAO@DMP[5] complex on the charge transport property of DAO after encapsulating with DMP[5], we studied the frontier molecular orbitals and surface electrostatic potential (ESP) properties of DAO and DAO@DMP[5]. Ground states of individual DAO and DAO@DMP[5] were relaxed at B3LYP/6–311(d, p). Their frontier molecular orbitals were shown in Fig. 4a, and the optimized geometries are shown in Fig. S11. The electrons were localized on both ends of the molecular skeleton due to the non-conjugated property of the alkyl chain (DAO). On the contrary, DMP[5] molecule showed high delocalization due to its high conjugated property. For the DAO@DMP[5] complex, the molecular orbitals of DMP[5] were the same, leading to the encapsulation with no effect on the conductance of DAO. Although the molecu-

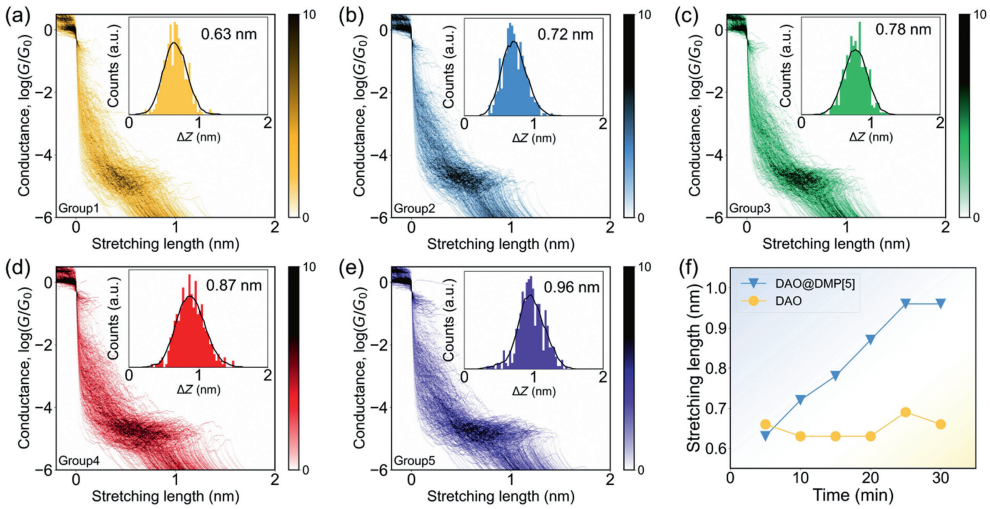

Fig. 3. Investigation on the dynamics of host-guest (DMP[5]-DAO) interaction. 2D conductance histograms for DAO and DMP[5] junctions constructed at five-minute intervals after mixing, and labeled them as (a) Group 1, (b) Group 2, (c) Group 3, (d) Group 4 and (e) Group 5, respectively. Insets: the corresponding relative displacement distribution of single-molecule junctions, which were calibrated with conductance region from $10^{-2.0}$ G_0 to $10^{-6.0}$ G_0 (775 nS to 0.08 nS), respectively. (f) Plots of the stretching length of the individual DAO and DAO@DMP[5] complex molecular junction with the measurement time, respectively.

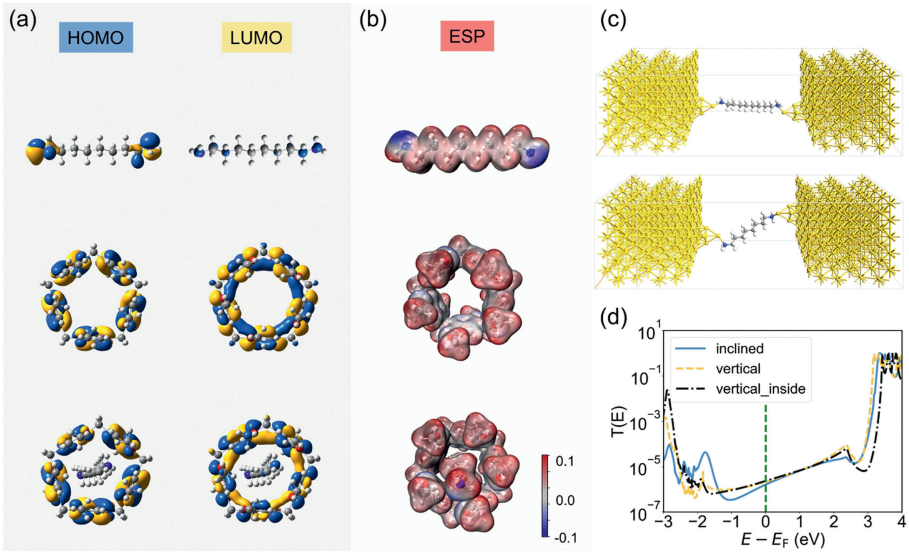

Fig. 4. Theoretical results. (a) Frontier molecular orbitals of DAO, DMP[5] and DAO@DMP[5] complex relaxed at the B3LYP/6–311(d, p) level. (b) ESP maps of DAO, DMP[5] and DAO@DMP[5] complex, the value on the colour bar is relative. (c) Molecular junction models correspond to two types of configurations of DAO. Top, vertical; bottom, inclined. (d) Transmissions at the zero bias. The item 'inclined' means DAO is inclined to the gold electrode, 'vertical' means DAO is perpendicular to the gold electrode, and 'vertical_inside' refers to DAO inserted into DMP[5].

lar orbitals of DAO changed around anchoring groups, that of DAO maintained the same at the backbone. For the optimized geometry, the DAO in the DAO@DMP[5] complex was significantly different from that of the induvial DAO. As shown in Fig. S9a, the DAO in the DAO@DMP[5] complex became spiral due to the interaction between DAO and DMP[5]. To quantify the interaction between molecules, we calculated the binding energy between DAO molecules and DAO-encapsulated DMP[5] molecules. As shown in Fig. S10 (Supporting information), the binding energy changed from −6.26 kcal/mol to +1.28 kcal/mol, indicating that the repulsive force between the DAO@DMP[5] complex further inhibited the interaction between DAO molecules.

We calculated the surface ESP to further validate the electrostatic interaction between DAO and DMP[5] molecules. As shown in Fig. 4b, the negative potential sites concentrate in amino groups of DAO and the cavity of DMP[5], indicating that DAO can be encapsulated by DMP[5] with an electrostatic effect. For the DAO@DMP[5] complex, ESP values have no change. Therefore, encapsulation has no effect on conductance. Based on the above results, the effect of DMP[5] on the conductance of DAO in the DAO@DMP[5] complex is not from the charge exchange, but the geometry change. Therefore, we simplified the DAO@DMP[5] to optimize DAO in DAO@DMP[5] in the transmission calculations. We performed the transmission spectra combining DFT and nonequilibrium Green's function method (NEGF) integrated within the Atomistix ToolKit (ATK) software package [55]. According to the results of molecular orbitals, we utilized the optimization model and calculated the transmission spectrum of DAO@DMP[5] complex by removing DMP[5] host. Firstly, we optimized the geometries of devices and subsequently performed their charge transport proper-

ties. The geometries are shown in Fig. 4c, and the detailed calculating information was provided in methods. DAO perpendicular to the gold electrode is analogous to the fully stretched state, and the length between the gold electrodes is longer than that of the incompletely stretched state. As shown in Fig. 4d, we performed the transmission spectra of three types of molecular junctions, $10^{-5.6}$ G_0 of vertical and vertical inside and $10^{-5.7}$ G_0 of inclined, indicating that the configurations had no effect on the charge transport.

To conclude, we developed a strategy based on the host-guest effect to decouple the interaction between the adjacent molecular chains. The molecular wires are constructed by DAO molecules, and DMP[5] molecules serve as insulating sheaths. The DAO@DMP[5] complex stabilized the molecular junctions and maintained the electrical conductance. The interaction among the DAO was suppressed *via* the steric effect of DMP[5], and the binding energy changes from −6.26 kcal/mol to +1.28 kcal/mol, which was confirmed by the increase of molecular lengths of the assembly complex of DAO and DMP[5] from 1.13 nm to 1.46 nm. The combined experimental and theoretical results revealed that DMP[5] with nanocavity can be used as a protective layer to relieve the intertwine of DAO in flexible chains. This work provides a new tactic to decouple the intermolecular and express the intrinsic molecular properties and thus promises high-density integrated molecular devices. The decoupling strategy similar to the cable structure may lead to wide applications in chemistry, material and electronics.

Declaration of competing interest

The authors declare that they have no known competing financial interests or personal relationships that could have appeared to influence the work reported in this paper.

CRediT authorship contribution statement

Saisai Yuan: Writing – review & editing, Writing – original draft, Funding acquisition, Data curation. **Yiming Chen:** Writing – original draft, Data curation. **Xijuan Wang:** Writing – review & editing, Data curation. **Degui Zhao:** Writing – review & editing. **Tengyang Gao:** Writing – review & editing, Funding acquisition. **Caiyun Wei:** Writing – review & editing. **Chuanxiang Chen:** Writing – review & editing. **Yang Yang:** Writing – review & editing, Funding acquisition. **Wenjing Hong:** Writing – review & editing, Funding acquisition, Conceptualization.

Acknowledgments

This work was supported by the National Natural Science Foundation of China (Nos. 22205084, 42307566, 22325303, 22250003, T2222002, 21991130, 22032004), Fujian Provincial Natural Science Foundation of China (No. 2022H6014), the China Postdoctoral Science Foundation (Nos. 2023M741039, 2023M742199), Project funded by National & Local Joint Engineering Research Center for Mineral Salt Deep Utilization (No. SF202303), State Key Laboratory of Efficient Utilization for Low Grade Phosphate Rock and Its Associated Resources WFKF (2023) 013, the Fundamental Research Funds for the Central Universities (Xiamen University, No. 20720240053), and State Key Laboratory of Vaccines for Infectious Diseases, Xiang An Biomedicine Laboratory (No. 2023XAKJ0103074).

Supplementary materials

Supplementary material associated with this article can be found, in the online version, at doi:10.1016/j.cclet.2025.110816.

References

[1] A.I. Yanson, G.R. Bollinger, H.E. van den Brom, N. Agraït, J.M. van Ruitenbeek, Nature 395 (1998) 783–785.
[2] M.A. Reed, C. Zhou, C.J. Muller, T.P. Burgin, J.M. Tour, Science 278 (1997) 252–254.
[3] D.J. Wold, C.D. Frisbie, J. Am. Chem. Soc. 123 (2001) 5549–5556.
[4] L. Zhang, E. Laborda, N. Darwish, et al., J. Am. Chem. Soc. 140 (2018) 766–774.
[5] B.F. Zeng, Y.L. Zou, G. Wang, et al., Nano Today 47 (2022) 101660.
[6] Y.L. Zou, Q.M. Liang, T. Lu, et al., Sci. Adv. 9 (2023) eadf0425.
[7] A. Zhang, X. Zhuang, J. Liu, et al., Nat. Catal. 6 (2023) 266–275.
[8] A.K. Ismael, K. Wang, A. Vezzoli, et al., Angew. Chem. Int. Ed. 56 (2017) 15378–15382.
[9] D.C. Milan, M. Krempe, A.K. Ismael, et al., Nanoscale 9 (2017) 355–361.
[10] P. Gehring, J.M. Thijssen, H.S.J. van der Zant, Nat. Rev. Phys. 1 (2019) 381–396.
[11] S. Yuan, Q. Zhang, Front. Chem. 9 (2021) 812287.
[12] M.W. Gu, H.H. Peng, I.W.P. Chen, C.H. Chen, Nat. Mater. 20 (2021) 658–664.
[13] B.F. Zeng, J.Y. Wei, X.G. Zhang, et al., Chem. Sci. 13 (2022) 7765–7772.
[14] B.F. Zeng, R. Deng, Y.L. Zou, et al., CCS Chem. 5 (2023) 830–840.
[15] J. Li, S. Hou, Y.R. Yao, et al., Nat. Mater. 21 (2022) 917–923.
[16] J. Bai, A. Daaoub, S. Sangtarash, et al., Nat. Mater. 18 (2019) 364–369.
[17] S. Wu, M.T. González, R. Huber, et al., Nat. Nanotechnol. 3 (2008) 569–574.
[18] R. Frisenda, V.A.E.C. Janssen, F.C. Grozema, H.S.J. van der Zant, N. Renaud, Nat. Chem. 8 (2016) 1099–1104.
[19] L. Venkataraman, J.E. Klare, C. Nuckolls, M.S. Hybertsen, M.L. Steigerwald, Nature 442 (2006) 904–907.
[20] E. Wierzbinski, X. Yin, K. Werling, D.H. Waldeck, J. Phys. Chem. B 117 (2013) 4431–4441.
[21] Y. Zang, Q. Zou, T. Fu, et al., Nat. Commun. 10 (2019) 4482.
[22] C.S. Quintans, D. Andrienko, K.F. Domke, et al., Appl. Sci. 11 (2021) 3317.
[23] H. Chen, Y. Li, S. Chang, Anal. Chem. 92 (2020) 6423–6429.
[24] M. Huang, L. Yu, M. Zhang, et al., Small 17 (2021) 2101911.
[25] W. Haiss, R.J. Nichols, H. van Zalinge, et al., Phys. Chem. Chem. Phys. 6 (2004) 4330–4337.
[26] C.A. Nijhuis, W.F. Reus, G.M. Whitesides, J. Am. Chem. Soc. 131 (2009) 17814–17827.
[27] L. Jiang, C.S.S. Sangeeth, C.A. Nijhuis, J. Am. Chem. Soc. 137 (2015) 10659–10667.
[28] C. Li, I. Pobelov, T. Wandlowski, et al., J. Am. Chem. Soc. 130 (2008) 318–326.
[29] X. Li, J. He, J. Hihath, et al., J. Am. Chem. Soc. 128 (2006) 2135–2141.
[30] H. Ju, J. Wang, W. Liu, et al., CCS Chem. 6 (2024) 2704–2712.
[31] B. Han, Y. Li, X. Ji, et al., J. Am. Chem. Soc. 142 (2020) 9708–9717.
[32] A. Feng, Y. Zhou, M.A.Y. Al-Shebami, et al., Nat. Chem. 14 (2022) 1158–1164.
[33] E.M. Cabaleiro-Lago, J. Rodríguez-Otero, ACS Omega 3 (2018) 9348–9359.
[34] L. Herrer, S. Naghibi, I. Marín, et al., Adv. Mater. Interfaces 10 (2023) 2300133.
[35] S. Yuan, Q. Qian, Y. Zhou, et al., Small 18 (2022) 2104554.
[36] Z. Wang, Y. Li, M. Sun, Phys. Chem. Chem. Phys. 26 (2024) 1067–1076.
[37] H. Ju, B. Wang, M. Li, et al., J. Am. Chem. Soc. 146 (2024) 25290–25298.
[38] L. Zhou, Y. Zhou, L. Fang, et al., Chin. Chem. Lett. 35 (2024) 109509.
[39] Y. Jia, W.L. Guan, J. Liu, et al., Chin. Chem. Lett. 34 (2023) 108082.
[40] C. Schönbeck, H. Li, B.H. Han, B.W. Laursen, J. Phys. Chem. B 119 (2015) 6711–6720.
[41] W.L. Guan, J.F. Chen, J. Liu, et al., Coord. Chem. Rev. 507 (2024) 215717.
[42] M. Xue, Y. Yang, X. Chi, Z. Zhang, F. Huang, Acc. Chem. Res. 45 (2012) 1294–1308.
[43] T. Ogoshi, T.A. Yamagishi, Y. Nakamoto, Chem. Rev. 116 (2016) 7937–8002.
[44] S. Bingbing, W. Yuchun, Z. Yi, et al., Chin. Chem. Lett. 35 (2024) 109540.
[45] C. Wang, L. Xu, Z. Jia, T.P. Loh, Chin. Chem. Lett. 35 (2024) 109075.
[46] B. Xu, N.J. Tao, Science 301 (2003) 1221–1223.
[47] N.L. Strutt, R.S. Forgan, J.M. Spruell, Y.Y. Botros, J.F. Stoddart, J. Am. Chem. Soc. 133 (2011) 5668–5671.
[48] C. Wu, D. Bates, S. Sangtarash, et al., Nano Lett. 20 (2020) 7980–7986.
[49] N. Agraït, A.L. Yeyati, J.M. van Ruitenbeek, Phys. Rep. 377 (2003) 81–279.
[50] W. Hong, H. Valkenier, G. Mészáros, et al., Beilstein. J. Nanotechnol. 2 (2011) 699–713.
[51] D. Su, S. Zhou, H. Masai, et al., Adv. Sci. 9 (2022) 2200022.
[52] O. Adak, E. Rosenthal, J. Meisner, et al., Nano Lett. 15 (2015) 4143–4149.
[53] S. Yuan, T. Gao, W. Cao, et al., Small Methods 5 (2021) 2001064.
[54] C. Tang, L. Chen, L. Zhang, et al., Angew. Chem. Int. Ed. 58 (2019) 10601–10605.
[55] M. Brandbyge, J.L. Mozos, P. Ordejón, J. Taylor, K. Stokbro, Phys. Rev. B 65 (2002) 165401.